Research in Astron. Astrophys. **2011** Vol. **11** No. **2**, 156–162
http://www.raa-journal.org *http://www.iop.org/journals/raa*

Research in Astronomy and Astrophysics

H_2CO and H110α survey toward UCHII regions *

Xiao-Hong Han[1,2], Jian-Jun Zhou[1], Jarken Esimbek[1], Gang Wu[1,2] and Ming-Fei Gao[1]

[1] National Astronomical Observatories / Urumqi Observatory, Chinese Academy of Sciences, Urumqi 830011, China; *hanxh@uao.ac.cn*
[2] Graduate University of Chinese Academy of Sciences, Beijing 100049, China

Received 2010 March 30; accepted 2010 August 12

Abstract We report results of the H_2CO and H110α survey toward 281 UCHII regions using the Urumqi 25m radio telescope. We obtained 37 new H_2CO detections, and H110α was simultaneously detected in eight of them. Only H110α was detected in another UCHII region. We calculated kinematic distances of nine UCHII regions with the detected H110α and resolved the kinematic distance ambiguity for six of them. The detection rate of H_2CO of our observation was 13.2%, which is low compared with one of the other authors. The possible reason is that the sensitivity of our telescope is relatively low.

Key words: ISM: HII regions — ISM: molecules — radio lines: ISM

1 INTRODUCTION

UCHII (Ultracompact ionized hydrogen) regions are manifestations of newly formed massive stars that are still embedded in their natal molecular clouds. They are good tracers of the spiral arms of the Galaxy (Churchwell 2002). If we know the distances of UCHII regions, we can determine their bolometric luminosity, mass and size, and these parameters can help constrain the theoretical models of star formation and evolution of molecular clouds. The establishment of distances to UCHII regions also provides an opportunity to improve our understanding of the large scale structure of the Galaxy.

The simplest and most common way to estimate the distance to a UCHII region with a measured velocity is to assume a Galactic rotation curve and calculate their kinematic distances. The known distances to almost all UCHII regions are kinematic distances because they are too heavily obscured to use any of the optical distance determination methods. Generally, the radial velocities of UCHII regions have been detected by observing their hydrogen radio recombination lines. However, if UCHII regions are located within the inner Galaxy (solar circle), the calculation will get one near distance and one far distance, which is called the kinematic distance ambiguity (KDA). There is no KDA for those UCHII regions located within the outer Galaxy. The distance ambiguity can be resolved by searching for absorption features against the continuum background (Fish et al. 2003). The KDA of many UCHII regions have been resolved by observing HI or H_2CO absorption lines (Araya et al. 2002; Fish et al. 2003; Andersen & Bania 2009).

Many UCHII regions have been found to date. Wood & Churchwell identified $\sim$ 1650 UCHII regions from IRAS point sources. White et al. (1991), Helfand et al. (1992) and Becker et al. (1994)

* Supported by the National Natural Science Foundation of China.

identified $\sim$ 770 UCHII regions based on the coincidence of IRAS point sources with thermal radio sources. Recently, Giveon et al. (2005a,b) identified $\sim$ 1240 UCHII regions based on the coincidence of MSX point sources with thermal radio sources. However, less than 150 UCHII regions have known distances (Anderson & Bania 2009). We plan to make an H110α and H_2CO line survey toward a large sample of UCHII regions within the inner Galaxy. We hope to simultaneously detect H110α and H_2CO toward UCHII regions, and resolve their KDA. Then we can study the Galactic structure and massive star formation properties based on these UCHII regions. Here we present our first H110α and H_2CO survey results. We describe our observations in Section 2. The observation results and discussion are presented in Section 3. Section 4 is a brief summary.

2 SAMPLE AND OBSERVATION

We selected 281 UCHII regions according to the following criteria: (1) They are located in the first quadrant of the Galaxy; (2) Their latitudes are above -30°; (3) Taking into consideration the beam size of the Urumqi 25 m radio telescope, we exclude those UCHII regions with angular separations less than 5 arcmin between each other. Most UCHII regions were selected from Giveon et al. (2005a,b), where they show strong mid-infrared radiation and radio radiation at centimeter wavelengths. In order to use the allotted observation time efficiently, we have to select some sources located in the outer Galaxy. Most such UCHII regions were selected from Wood & Churchwell (1989). In addition, W51, a source with strong H110α and H_2CO lines (Downes et al. 1980), was observed during each observation to test whether the system worked well.

Our observations were made from 2008 September to 2009 September and from 2010 May to 2010 July with the 25 m radio telescope of Urumqi Observatory. This telescope was built in 1993 as an element of the Chinese Very Long Baseline Interferometry network. It is located in the Nanshan mountains west of Urumqi city at an altitude of 2080 m. Its front-end receiver system includes several receivers working at different wavelengths, such as λ= 18, 13, 3.6 and 6 cm. One digital autocorrelation spectrometer with 4096 channels was installed on the back-end, whose maximum bandwidth is 80 MHz. The 6 cm receiver is a cryogenic receiver with noise temperature $\sim$ 23 K. The main beam efficiency is $\sim$65% at 6 cm. We simultaneously observed H110α at 4874.157 MHz and H_2CO at 4829.6594 MHz with an 80 MHz bandwidth, corresponding to spectral resolution 19.5 kHz. Position-switching mode was adopted for our observation. The weather was usually good during our observations. A diode noise tube was used to calibrate the spectrum. The flux error was $\sim$15%, and the DPFU (Degrees Per Flux Unit) was 0.116 K Jy^{-1} at a wavelength of 6 cm for our telescope.

3 RESULTS AND DISCUSSIONS

We simultaneously observed H_2CO and H110α toward 281 UCHII regions, and found that H_2CO was newly detected toward 37 sources, and H110α was simultaneously detected in eight of them. Only H110α was detected toward another UCHII region. The detection rate of H_2CO was about 13.2%. The reason for a low detection rate may be that the intensity of H_2CO is weak and the sensitivity of our telescope is low. The data were reduced with the GILDAS software package developed by IRAM, and the H110α and H_2CO line parameters were derived by fitting Gaussian profiles to each velocity component along the line of sight. The observation result of W51 is consistent with previous results (Downes et al. 1980), which indicates that the system worked well.

In 29 sources, only H_2CO absorption lines were detected (see Table 1 and Fig. 1). In Table 1, Col. (1) lists the source name, and Cols. (2) and (3) list the source coordinates. Columns (4), (5) and (6) list LSR velocity, line width and intensity of H_2CO spectral features respectively. The errors quoted in parentheses are the formal 1-σ errors of the fits. The H_2CO absorption lines are displayed in Figure 1. Most UCHII regions show only one absorption feature. Only G8.6614–0.3434 and G33.4178–1.2128 display two and three absorption features, respectively. This indicates that there are several molecular clouds with different velocities along the line of sight of these two

Table 1 Coordinates and Line Parameters of 29 UCHII Regions with the H_2CO Line Detected

Source	α (J2000) (h m s)	δ (J2000) (° ′ ″)	$V_{\rm lsr}$ (km s^{-1})	FWHM (km s^{-1})	Intensity (Jy)
(1)	(2)	(3)	(4)	(5)	(6)
G2.8930 + 0.0243	17 52 15.60	−26 26 38.40	6.961 (1.111)	35.542 (2.803)	−1.389 (0.325)
G8.6614 − 0.3434	18 06 15.29	−21 37 35.76	16.809 (0.207)	2.306 (0.464)	−0.957 (0.294)
			34.975 (0.205)	4.526 (0.501)	−1.356 (0.223)
G22.7253 − 0.0106	18 32 42.16	−09 04 42.96	74.088 (0.702)	7.591 (2.608)	−0.433 (0.132)
G33.4178 − 0.0038	18 52 20.28	00 25 50.88	9.680 (0.185)	2.216 (0.320)	−0.592 (0.116)
			71.800 (0.373)	5.161 (0.951)	−0.418 (0.120)
			102.069 (0.428)	6.770 (1.248)	−0.403 (0.118)
G35.1387 − 0.7622	185810.70	01 36 57.60	33.748 (0.185)	4.420 (0.436)	−1.198 (0.127)
G39.7279 − 0.3974	19 05 18.00	05 51 47.16	58.576 (0.502)	4.134 (0.893)	−0.351 (0.105)
G39.8821 − 0.3457	19 05 24.02	06 01 25.68	58.450 (0.298)	6.206 (0.639)	−0.449 (0.071)
G41.1984 + 0.0356	19 06 28.29	07 22 05.16	39.835 (0.387)	5.230 (0.831)	−0.377 (0.095)
G75.7666 + 0.3424	20 21 41.47	37 25 51.20	0.970 (0.750)	8.109 (2.297)	−0.557 (0.179)
G76.1877 + 0.0974	20 23 55.17	37 38 10.30	0.946 (0.354)	4.891 (0.810)	−0.367 (0.075)
G80.8645 + 0.4197	20 36 52.27	41 36 23.70	−1.587 (0.275)	3.322 (1.104)	−0.563 (0.106)
G80.9383 − 0.1268	20 39 25.80	41 20 01.68	7.656 (0.158)	2.060 (0.264)	−0.661 (0.082)
G105.6270 + 0.3388	22 32 45.76	58 28 19.20	−50.248 (0.484)	4.292 (0.978)	−0.174 (0.052)
G110.1082 + 0.0473	23 05 10.34	60 14 46.30	−49.848 (0.154)	3.443 (0.360)	−0.698 (0.044)
IRAS 03225 + 3034	03 25 35.90	03 45 17	6.909 (0.119)	1.829 (0.542)	−0.901 (0.111)
IRAS 03245 + 3002	03 27 39.10	03 13 01	7.823 (0.096)	1.675 (0.334)	−1.967 (0.185)
IRAS 04067 + 3954	04 10 08.40	40 02 24	−2.330 (0.141)	2.053 (0.298)	−0.819 (0.102)
IRAS 04271 + 3502	04 30 25.80	35 09 13	2.122 (0.307)	3.264 (0.571)	−0.529 (0.109)
IRAS 04381 + 2540	04 41 12.48	25 46 37.1	7.245 (0.103)	1.873 (0.198)	−1.541 (0.225)
IRAS 05155 + 0707	05 18 17.47	07 10 58.4	−0.689 (0.104)	2.237 (0.210)	−0.796 (0.065)
IRAS 05271 + 3059	05 30 21.20	31 01 27	−18.840 (0.300)	2.408 (0.670)	−0.789 (0.193)
IRAS 05283 − 0412	05 30 51.60	−04 09 31	11.907 (0.157)	1.965 (0.456)	−0.871 (0.119)
IRAS 05351 + 3549	05 38 28.10	35 51 15	−18.784 (0.296)	3.565 (0.544)	−0.702 (0.136)
IRAS 05496 + 0812	05 52 22.50	08 13 34	51.941 (1.996)	5.196 (3.886)	−0.468 (0.122)
IRAS 06047 + 2040	06 07 45.20	20 39 38	7.732 (0.176)	1.867 (0.430)	−0.948 (0.187)
IRAS 06084 − 0611	06 10 50.20	−06 12 01	10.449 (0.471)	3.218 (1.025)	−0.624 (0.188)
IRAS 06381 + 1039	06 40 58.00	10 36 49	10.471 (0.418)	3.372 (0.894)	−0.640 (0.194)
IRAS 07060 − 1026	07 08 27.50	−10 31 27	13.498 (0.192)	3.769 (0.419)	−0.475 (0.062)
IRAS 07077 − 1026	07 10 05.40	−10 31 46	13.551 (0.094)	2.737 (0.204)	−1.596 (0.115)

Notes: The errors quoted in parentheses are the formal 1-σ errors of the fits.

UCHII regions. However, similar observations with larger radio telescopes usually detect multiple absorption features toward UCHII regions (Sewilo et al. 2004). A reasonable interpretation is that the sensitivity of our telescope is too low to detect very weak features. G2.8930+0.0243 shows one very wide spectral feature, if we take into consideration that CO clouds in this region show very large line width (Oka et al. 1998). If there exists a good correlation between H_2CO absorption and CO emission (Rodriguez et al. 2006), such a large line width might be explained.

Table 2 gives the line parameters of these eight UCHII regions with both H_2CO and H110α detected and one UCHII with only H110α detected. It includes the coordinates, LSR velocity, line width and intensity of H_2CO and H110α lines, where the errors quoted in parentheses are the formal 1-σ errors of the fits. Here we also list the parameters of W51 (G49.4860–0.3813) in Table 2 to compare with previous results. Figure 2 displays their spectra. We can see from Table 2 that the H_2CO absorption lines have nearly the same velocities as that of the hydrogen emission line, which demonstrates that these UCHII regions are associated with molecular clouds (Araya et al. 2002). The H110α line width of the source G35.5423+0.0038 is less than 16 km s^{-1}, which may be due to the low signal to noise ratio of the spectra.

We present the kinematic distances derived from the rotation curve of Reid (2009) in Table 3, corresponding to $R_0 = 8.4$ kpc and $\Theta_0 = 254$ km s^{-1}. We followed the method of Sewilo et

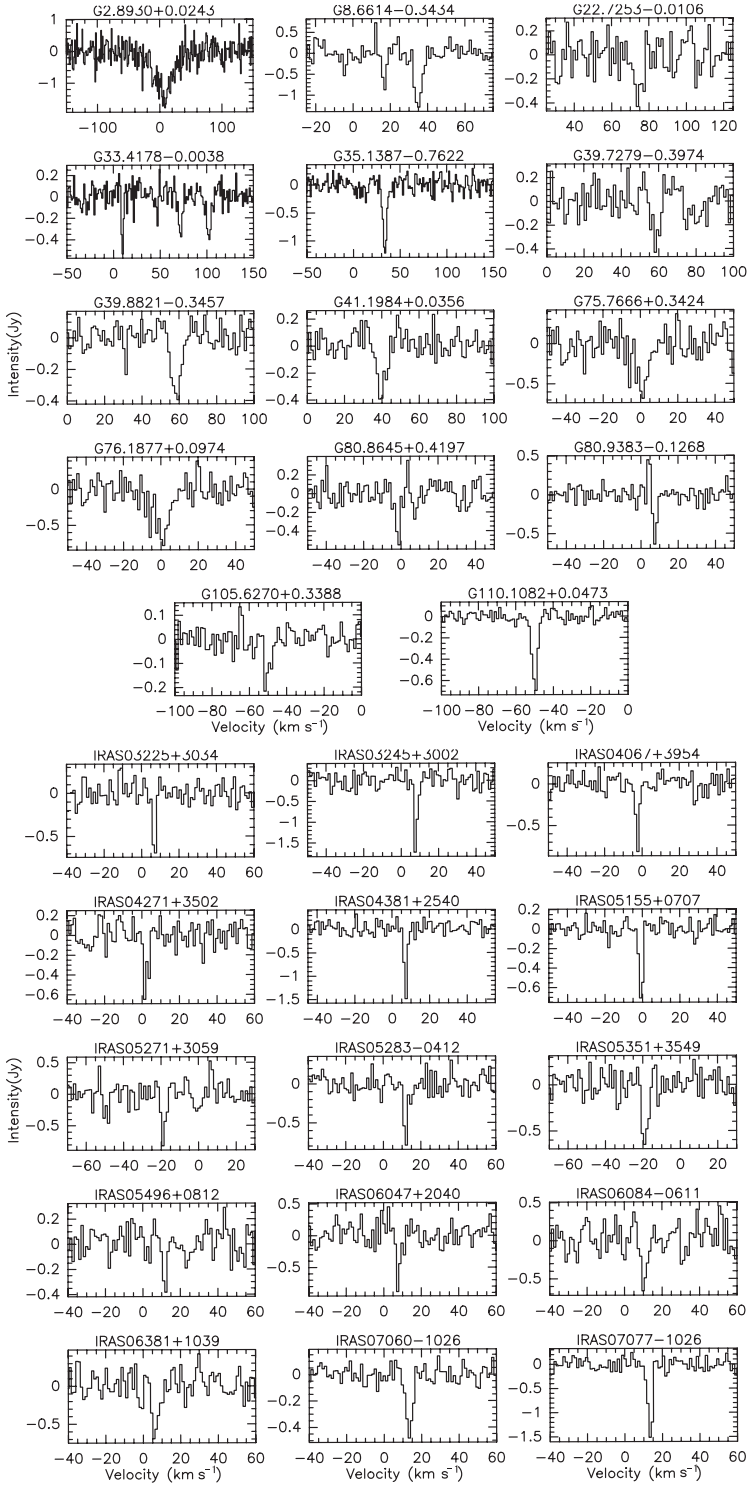

Fig. 1 H_2CO absorption lines observed toward 29 UCHII regions. The source name is labeled on the top of each panel.

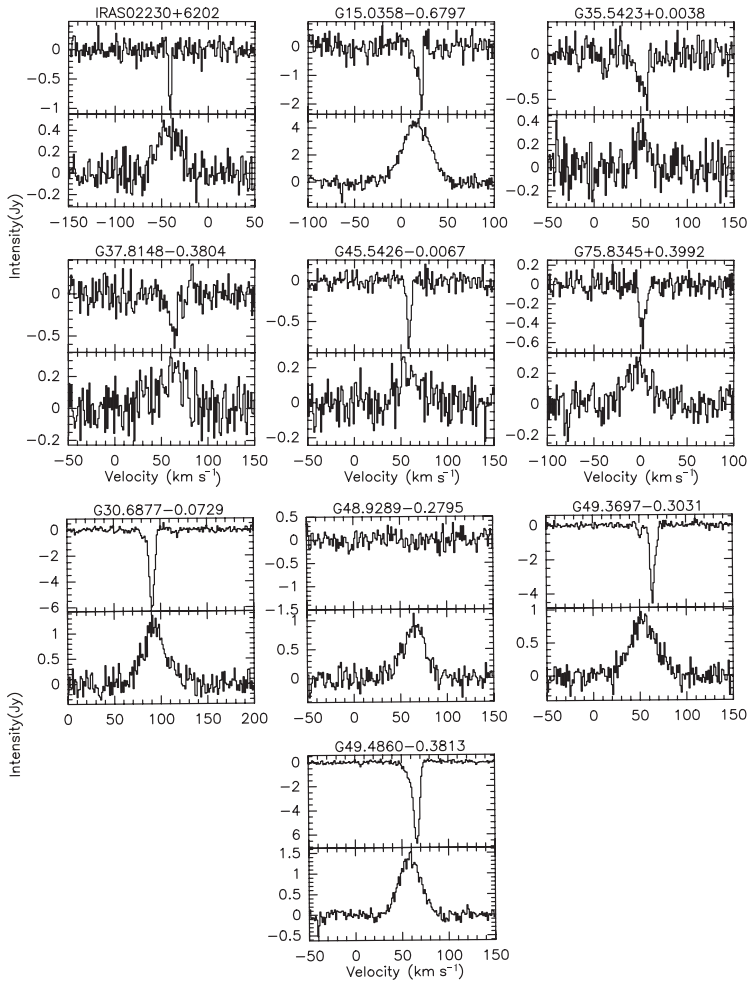

Fig. 2 Spectra of H_2CO (*upper two row panels*) and H110α (*lower two row panels*) observed toward ten UCHII regions. The source name is labeled on the top of each panel.

al. (2004) to resolve the KDA of these sources. For the sources G48.9289–0.2795, G49.3697–0.3031 and G49.4860–0.3813 (W51), $|V_{\rm HIIregion}| > |V_{\rm tp}|$. We followed the suggestion of Sewilo et al. (2004) and classified them at the tangent point. This was supported by the fact that we obtained the same near and far distances. If the H_2CO line velocity lies between the source velocity ($|V_{\rm HIIregion}|$) plus 10 km s^{-1} and the LSR velocity at the tangent point ($|V_{\rm tp}|$) plus 10 km s^{-1}, and ($|V_{\rm HIIregion}|$+ 10 km s^{-1}) $< |V_{\rm tp}|$, we classified the source as a far distance one. Otherwise, the near distance was assigned. We thus classified sources G15.0358–0.6797, G37.8148–0.3804 and G35.5423+0.0038 as located at the near distances. For the sources G30.6877–0.0729, G45.5426–0.0067 and G75.8345+0.3992, because they satisfy the condition ($|V_{\rm tp}|-10$ km s^{-1})$<|V_{\rm HIIregion}| < |V_{\rm tp}|$, we cannot unambiguously distinguish between the near and far positions of the source. Since the source IRAS 02230+6202 is located in the second quadrant of the Galaxy, there is no KDA, so only one value is available, and thus adopted. This source also has no $V_{\rm tp}$. Keeping in mind, for

Table 2 Coordinates and Line Parameters of Nine UCHII Regions with H110α and H_2CO Detected and One UCHII Region with only H110α Detected

Source	α (J2000)	δ (J2000)	H_2CO			H110α		
			$V_{\rm lsr}$	FWHM	Intensity	$V_{\rm lsr}$	FWHM	Intensity
	(h m s)	(° ′ ″)	(km s^{-1})	(km s^{-1})	(Jy)	(km s^{-1})	(km s^{-1})	(Jy)
(1)	(2)	(3)	(4)	(5)	(6)	(7)	(8)	(9)
G15.0358–0.6797	18 20 25.5	–16 11 35.52	20.96(0.577)	4.891(1.490)	–1.95(0.280)	16.30(0.298)	34.84(0.692)	4.35(0.288)
G30.6877–0.0729	18 47 36.19	–02 01 49.44	90.98(0.057)	6.511(0.139)	–6.01(0.177)	93.02(0.58)	28.91(1.50)	1.10(0.155)
G35.5423+0.0038	18 56 11.3	02 19 29.28	52.26(0.856)	13.38(2.180)	–0.408(0.125)	51.50(1.32)	15.08(2.72)	0.273(0.122)
G37.8148–0.3804	19 01 43.10	04 10 14.52	62.64(0.658)	9.540(2.200)	–0.487(0.132)	61.90(2.54)	33.76(8.02)	0.217(0.106)
G45.5426–0.0067	19 14 45.72	11 12 03.96	58.64(0.153)	4.527(0.372)	–0.784(0.074)	58.64(1.75)	25.06(4.22)	0.176(0.077)
G48.9289–0.2795	19 22 14.80	14 03 58.32				64.77(0.591)	27.90(1.44)	0.888(0.129)
G49.3697–0.3031	19 23 11.47	14 26 37.3	50.66(0.240)	3.858(0.582)	–0.743(0.120)	53.71(0.592)	32.82(1.41)	0.817(0.111)
			64.23(0.056)	6.087(0.143)	–4.13(0.120)			
G49.4860–0.3813[a]	19 23 42.09	14 30 33.3	65.83(0.051)	8.108(0.129)	–6.55(0.148)	58.33(0.266)	26.84(0.602)	1.37(0.093)
G75.8345+0.3992	20 21 39.04	37 31 08.76	2.335(0.335)	7.241(0.733)	–0.50(0.081)	–2.968(1.45)	31.15(3.54)	0.224(0.076)
IRAS 02230+6202	02 26 51.14	62 15 47.2	–40.92(0.143)	2.848(0.292)	–1.11(0.123)	–42.950(1.07)	27.29(2.24)	0.409(0.109)

Notes: The errors quoted in parentheses are the formal 1-σ errors of the fits. [a] G49.4860–0.3813 is the source W51.

Table 3 Kinematic Parameters Derived from the Galactic Rotation Curve of Reid (2009)

Source	$\lvert V_{\rm HII\ region}\rvert$ (km s^{-1})	$V_{\rm tp}$ (km s^{-1})	$R_{8.4}$ (kpc)	$D_{n8.4}$ (kpc)	$D_{f8.4}$ (kpc)	Note
(1)	(2)	(3)	(4)	(5)	(6)	(7)
G15.0358–0.6797	16.30	151.704	6.56	1.97	14.45	N
G30.6877–0.0729	93.02	102.176	4.72	5.39	9.23	
G35.5423+0.0038	51.50	87.679	6.05	3.35	10.48	N
G37.8148–0.3804	61.90	81.137	5.83	4.01	9.42	N
G45.5426–0.0067	58.64	60.298	6.16	4.61	7.30	
G48.9289–0.2795	64.77	51.943	6.33	5.58	5.58	T
G49.3697–0.3031	53.71	50.894	6.38	5.53	5.53	T
G49.4860–0.3813[a]	58.33	50.618	6.39	5.52	5.52	T
G75.8345+0.3992	2.968	6.674	8.34	0.27	3.89	
IRAS 02230+6202	42.95		10.89	3.32	3.32	O

Notes: R stands for the distance from the source to the Galactic center. $V_{\rm tp}$ is the LSR velocity of the tangent point. "T" stands for the distance to the tangent point. "O" denotes only one kinematic distance of a UCHII region when it is located in the outer Galaxy. When a UCHII region is located in the inner Galaxy, one near kinematic distance and one far kinematic distance are available. "N" represents that the near distance is adopted, and F represents that the far distance is adopted. $D_{n8.4}$ stands for the near distance, $D_{f8.4}$ stands for the far distance. [a] G49.4860–0.3813 is the source W51.

those sources with the Galactic longitude near $l = 0°$ or 180°, the expected velocity (for circular rotation) is near nero, and the velocity uncertainty due to random motions has a large influence on the circular rotation velocity (Clemens 1985; Brand & Blitz 1993), so the kinematic distance of G15.0358–0.6797 suffers large uncertainties. For the source G75.8345+0.3992, whose LSR velocity is small, the contribution of peculiar motion deviations from circular rotation to the velocity may become important. Its kinematic distance also suffers an uncertainty.

4 SUMMARY

Using the Urumqi 25 m radio telescope, we observed H110α recombination lines and H_2CO absorption lines toward 281 UCHII regions. We found 37 new H_2CO sources, while H110α was simultaneously detected in eight of them. Only the H110α recombination line was detected toward another

one of the UCHII regions. The detection rate of our observation was about 13.2%; this is low compared with the observations of other authors (Araya et al. 2002; Sewilo et al. 2004). The probable reason is that the intensity of H_2CO is weak and the sensitivity of our telescope is relatively low. We calculated kinematic distances of nine UCHII regions with the detected H110α and we resolved the KDA for six of them.

Acknowledgements We thank Li-Gang Hou for his help in calculating the kinematic distances of UCHII regions. This work was funded by the National Natural Science Foundation of China (Grant Nos. 10873025 and 10778703) and the Program of Light in China's Western Region (LCRW) (Nos. RCPY200605 and RCPY200706).

References

Anderson, L. D., & Bania, T. M. 2009, ApJ, 690, 706
Araya, E., Hofner, P., Churchwell, E., & Kurtz, S. 2002, ApJS, 138, 63
Becker, R. H., White, R. L., Helfand, D. J., & Zoonematkermani, S. 1994, ApJS, 91, 347
Brand, J., & Blitz, L. 1993, A&A, 275, 67
Churchwell, E. 2002, ARA&A, 40, 27
Clemens, D. P. 1985, ApJ, 295, 422
Downes, D., Wilson, T. L., Bieging, J., & Wink, J. 1980, A&AS, 40, 379
Fish, V. L., Reid, M. J., Wilner, D. J., & Churchwell, E. 2003, ApJ, 587, 701
Giveon, U., Becker, R. H., Helfand, D. J., & White, R. L. 2005a, AJ, 129, 348
Giveon, U., Becker, R. H., Helfand, D. J., & White, R. L. 2005b, AJ, 130, 156
Helfand, D. J., Zoonematkermani, S., Becker, R. H., & White, R. L. 1992, ApJS, 80, 211
Oka, T., Hasegawa, T., Sato, F., Tsuboi, M., & Miyazaki, A. 1998, ApJS, 118, 455
Reid M. J., Menten, K. M., Zheng, X. W., Brunthaler, A., et al. 2009, ApJ, 700, 137
Rodriguez, M. I., Allen, R. J., Loinard, T., & Wiklind, T. 2006, ApJ, 652, 1230
Sewilo, M., Watson, C., Araya, E., Churchwell, E., Hofner, P., & Kurtz, S. 2004, ApJS, 154, 553
White, R. L., Becker, R. H., & Helfand, D. J. 1991, ApJ, 371, 148
Wood, D. O. S., & Churchwell, E. 1989, ApJ, 340, 265